Cluster-model study of CO adsorption on the Pt(111) surface

Shuhei Ohnishi
NEC Fundamental Research Laboratories, Miyukigaoka 34, Tsukuba, Ibaraki 305, Japan

Noriko Watari
NEC Scientific Information Systems Development Ltd., KSP R&D Bldg. Sakato 3-2-1, Kawasaki, Kanagawa 213, Japan
(Received 8 February 1993; revised manuscript received 28 December 1993)

Mechanism of CO chemisorption on a metal surface is discussed on the basis of self-consistent local-density-functional calculations using norm-conserving pseudopotential in the linear-combination-of-atomic-orbitals method. The CO/Pt(111) system is studied by the cluster model for metal surfaces by introducing a model potential intended to pick up surface states by placing dangling bonds around the cluster surface. The CO-2π state is found to lie about 2–4 eV above the Fermi level with weak bonding surface Pt atoms. The donation–back-donation mechanism is found to be unlikely in CO/Pt(111).

I. INTRODUCTION

CO adsorption to metal surface is one of the most intensively studied systems experimentally. Above all, the adsorption of CO on Pt(111) has been extensively investigated by many experiments such as ultraviolet photoelectron spectroscopy (UPS),[1–4] inverse ultraviolet photoelectron spectroscopy,[5–7] infrared (IR) spectroscopy,[8,9] low-energy electron diffraction,[10,11] electron-energy-loss spectroscopy,[12,13] core-photoionization spectra,[14,15] Auger spectra,[16] and the He-atom scattering experiment.[17,18] The mechanism of CO adsorption, however, has not yet been elucidated: the basic question on the difference between the dissociative and nondissociative adsorption was not clarified. The model widely accepted is the donation–back-donation one proposed by Blyholder,[19] in which the CO-metal bonding is described as arising from electron transfer from the CO-5σ orbital to unoccupied metal orbitals accompanied with back-donation from occupied metal orbitals to CO-2π orbital. Ishii, Ohno, and Viswanathan,[20] however, pointed out the inadequacy of Blyholder's model on the basis of recent spectroscopy measurements, which predicted no 2π state below the Fermi level. Theoretical studies focused on this point have not yet been done thoroughly on the basis of the first-principles calculation. Semiempirical analyses for experimental data by various theoretical models have provided us with information to understand basic geometrical and electronic structures of the CO/Pt system.[21–27] The relevant problem associated with the interaction between CO and transition-metal surfaces have been extensively discussed by the first-principles calculations by the cluster-model approach for metal surface.[25,28–33] Computational effort, therefore, has been mainly devoted to investigating cluster size and shape dependencies of electronic structures. Post and Baernds[28] performed a series of calculations by changing the cluster size and site for CO/Cu(100) and CO/Cu(111) systems with the Cu cluster of up to Cu_7. Small cluster-model calculations, however, gave information on the local σ bonding but indistinct delocalized nature of the π back-bonding and also site preferences of CO. For the CO/Cu(100) system, Bagus, Hermann, and Bauschlicher[29] and Hermann, Bagus, and Nelin[30] pointed out the possibility of an electron-transfer mechanism from Cu to CO-2π back-donation on the basis of the detailed analysis of the cluster-size dependence with model clusters from Cu_5 to Cu_{13}. For the other CO-metal interaction, Allison and Goddard[31] calculated the system of CO at the on-top site of the Ni(100) surface with the model cluster of Ni_{14}. They found a weak π contribution to the dipole moment of CO on Ni(100). Pavao *et al.*[32] discussed the charge transfer from Fe to CO by the model cluster of Fe_5CO for the CO/Fe(100) system, which is considered to be related to the dissociation mechanism. Pacchioni and Bagus[33] discussed the adsorption of CO on the bridge site of the Pd(100) surface with the Pd_8 cluster. In the Pd(100) case, the 2π back-donation effect was found to be weaker than that in the Cu and Ni metal surfaces. Gavezzotti, Tantardini, and Miessner[25] calculated the Pt_7CO cluster using the optimized relativistic pseudopotential. Their result supported the charge transfer from Pt to CO-2π. For the CO-Pt surface interaction, theoretical model studies[23,24] using IR reflection-adsorption spectroscopy and IR linewidth of the C-O stretching vibration led to the conclusion that the CO-Pt metal bond is weak and the dominant contribution comes from the CO-5σ orbital. Understanding the experimental data of comprehensive photoelectron spectroscopy, however, requires quantitative theoretical data determined by the first-principles calculation of electronic structures associated with the donation–back-donation mechanism.

In order to study the electronic structure in the local chemisorption of molecules on the metal surface, however, the cluster-model approach by the standard linear-combination-of-atomic-orbitals (LCAO) scheme is the most effective method to focus on the chemical bonding between the surface atom and molecule. There are, however, two difficulties in this approach. One is the problem associated with the atomic basis function: for a heavy element like Pt, the straightforward application of the LCAO scheme does not work well because of too many

atomic orbitals for basis function and the intractable radial nodes in the valence orbitals, as shown in Fig. 1(a). The other one is the termination problem associated with the cluster-model approach: the small cluster model cannot simulate the solid surface because of the free boundary condition for the surface of the model cluster. The first problem is overcome by the introduction of the norm-conserving pseudopotential[34] into the LCAO scheme, denoted by LCPSAO method[35] hereafter. It makes numerical calculation feasible enough to deal with any atom system because of the effective core potential determined by solving the Dirac equation self-consistently and the nodeless feature of radial wave function. For the second one, we have introduced the effective model potential,[35,36] expressed by $\hat{V}_M$ for terminating the cluster boundary. The model potential is constructed by the local potential with the projection operator by local atomic orbitals, which works to fix the dangling bonds of peripheral atoms in the cluster surface to the bulklike states.

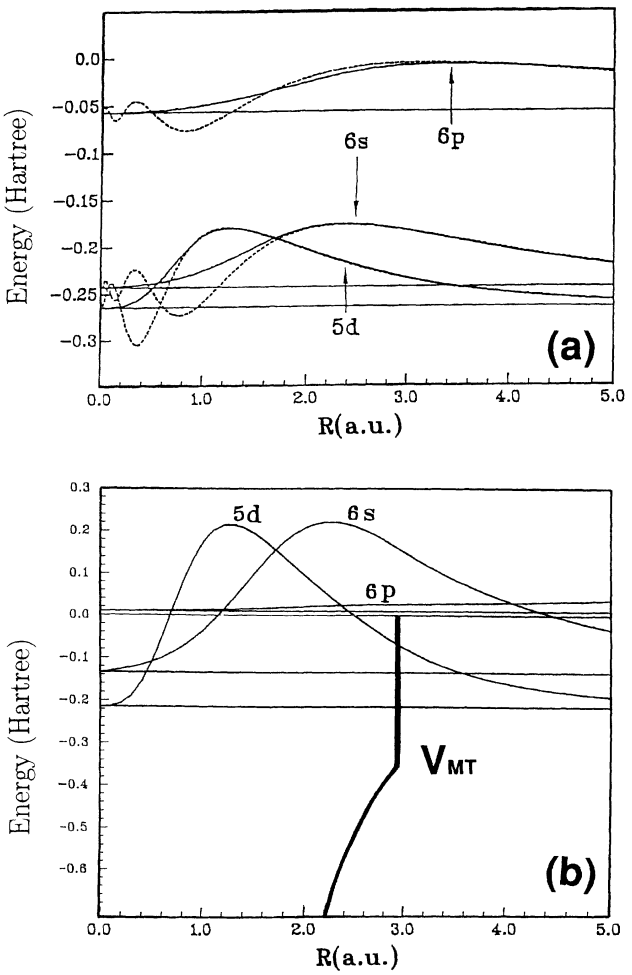

FIG. 1. Radial wave function of Pt. Horizontal lines indicate eigenvalues. (a) Free atom Pt. Solid and dotted curves are radial wave functions for the norm-conserving pseudopotential and full relativistic solutions, respectively. (b) Muffin-tin potential and radial wave functions. Since the 6p state does not have a bound-state solution, the wave function is given by the solution at the positive energy close to zero.

In this work, systems of CO on top site chemisorption on Pt(111) surface were modeled by clusters of $CO/Pt_{13}V_{M37}$. Computational details are discussed in Sec. II. In Sec. III, electronic structures are discussed on the basis of the self-consistent calculations within the local-density-functional scheme[37–40] by the LCPSAO method. Discussions concerning the effects of adsorption sites, atomic basis functions, and the effective model potential on electronic structures are given in Sec. IV. Site dependencies are studied by the model clusters of $CO/Pt_{19}V_{M42}$ and $CO/Pt_{22}V_{M52}$ for bridge and hollow pocket sites, respectively.

II. MODELS AND CALCULATIONS

A. Method

The LCPSAO-cluster method is characterized by the introduction of two effective potentials into the standard LCAO method. One is the norm-conserving pseudopotential for the atomic-core potential. The other one is the model potential, which is intended to be consistent with boundary conditions for the cluster. The total Hamiltonian for the present system is given by that of the free cluster under the external model potential $\hat{V}_{\rm ext}$,

$$H=[-\tfrac{1}{2}\Delta+\Sigma_i \hat{V}_{il}^{\rm ps}(\mathbf{r}-\mathbf{R}_i)+V_{\rm val}(\mathbf{r})+\hat{V}_{\rm ext}] , \quad (1)$$

where $\mathbf{R}_i$ is the atomic site. $\hat{V}_{il}^{\rm ps}$ is the effective core potential for atoms located at the site $\mathbf{R}_i$.

$$\hat{V}_l^{\rm ps}(r)=\hat{V}_l^{\rm ion}(r)+V_{\rm core}(r) , \quad (2)$$

$$\hat{V}_l^{\rm ion}(r)=|l\rangle\Delta V^{\rm ion}(r)\langle l| , \quad (3)$$

where $r=|\mathbf{r}|$. $V_{\rm val}$ is the sum of Coulomb potential V_C and the exchange-correlation potential given by the functional derivative of the exchange energy $E_{\rm XC}$ by the electron charge density ρ, as $V_{\rm XC}=\delta E_{\rm XC}/\delta\rho$. $E_{\rm XC}[\rho]$ is given by the standard local-density-functional formalism.[37–40]

$$V_{\rm val}(\mathbf{r})=V_C(\mathbf{r})+V_{\rm XC}(\mathbf{r}) . \quad (4)$$

The molecular orbital Ψ_ν at the eigenstate ν is given by the linear combination of symmetrized basis functions of atomic orbitals $\phi_{lm}(\mathbf{r})=\chi_l(r)Y_{lm}(\theta,\phi)$. The atomic radial wave function $\chi_l(r)$ and eigenvalue ε_l are given by solving the Kohn-Sham equation[37,38] self-consistently by introducing the norm-conserving pseudopotential for the effective core potential instead of solving core electronic states,

$$[-\tfrac{1}{2}\Delta+\hat{V}_l^{\rm ps}(\mathbf{r})+V_{\rm val}(\mathbf{r})]\phi_{lm}(\mathbf{r})=\varepsilon_l\phi_{lm}(\mathbf{r}) . \quad (5)$$

Figure 1(a) shows the nodeless feature of the radial wave function of Pt. The key technique in the LCPSAO method is the numerical one-center expansion of these smooth basis functions by applying the efficient Gauss-type cubature formula for a spherical surface determined on the basis of the group theoretical treatment,[41–45]

$$\phi_{ilm}=\phi_{lm}(\mathbf{r}-\mathbf{R}_i)=\Sigma_{l'm'}\xi_{ilm}^{l'm'}(r)Y_{l'm'}(\theta,\phi) , \quad r\le R_{\rm max} , \quad (6)$$

where $\xi_{ilm}^{l'm'}(r)$ is given by

$$\xi^{l'm'}_{ilm}(r)=\int \phi_{ilm}(\mathbf{r}-\mathbf{R}_i)Y_{l'm'}(\theta,\phi)d\Omega \ . \quad (7)$$

Matrix elements for the nonlocal potential term are calculated by these partial wave components as

$$\langle \phi_{i''l''m''}|\hat{V}^{\rm ion}_l|\phi_{i'l'm'}\rangle = \Sigma_m \int \xi^{lm}_{i''l''m''}(r)\Delta V^{\rm ion}_l(r)\xi^{lm}_{i'l'm'}(r)r^2dr \ . \quad (8)$$

$R_{\rm max}$ is about 2.5 a.u. for $\Delta V^{\rm ion}_l$. By solving the secular equation, molecular eigenvalues ε_ν, eigenfunctions Ψ_ν, and the total charge density $\rho=\Sigma_\nu f_\nu|\Psi_\nu|^2$ are determined self-consistently on the basis of the local-density-functional scheme. f_ν is the occupation number at the state ν. ρ is decomposed into the sum of nonspherical atomlike charge densities, ρ_{ilm}, $(l\le 4)$ located at each atom by the standard numerical-fitting procedure so as to be able to calculate the Coulomb potential energy accurately,[46-50]

$$\rho(\mathbf{r})\cong\Sigma_{ilm}\rho_{ilm}(\mathbf{r}-\mathbf{R}_i) \ , \quad (9)$$

where the radial part of $\rho_{ilm}(r)$ is given by all possible combinations of $\chi_{l'}(r)$ and $\chi_{l''}(r)$ multiplied by an auxiliary function to increase the number of fitting basis functions. All calculations have been done by using the minimal basis sets: $2s2p$ for C and O, $5d6s6p$ for Pt. The effects of additional basis function on electronic structures are discussed in Sec. IV. The number of sampling points is about 10 000/atom. The total energy $E_{\rm tot}$ is given by

$$E_{\rm tot}=\Sigma_\nu f_\nu\varepsilon_\nu-\tfrac{1}{2}\int\rho V_c d\mathbf{r}+E_{\rm XC}-\int\rho V_{\rm XC}d\mathbf{r} + \tfrac{1}{2}\Sigma'_{ij}Z_iZ_j/|\mathbf{R}_i-\mathbf{R}_j| \ . \quad (10)$$

The last term is the electrostatic energy of the nuclear charges without core electrons within the frozen-core approximation. Binding energy $-E_b$ is given by subtracting the sum of the total energy of the free surface cluster and molecule, as

$$E_b=E_{\rm tot}-(E_{\rm surf}+E_{\rm mol}) \ . \quad (11)$$

B. Effective model potential

The termination problem in the cluster-model approach is one of the most difficult problems in studying the localized electronic structures in bulk crystal and surface. Taking bigger cluster size to reduce the influence of the size effects on the focused region increases free boundary atoms responsible to cluster surface states, which induces the wrong energy-level sequence for occupied orbitals. The confinement of the spatial boundary with proper boundary conditions for wave functions and the electrostatic potential field causes many calculative difficulties in the LCAO scheme. The simple potential field given by superimposed charge densities of surrounding atoms cannot provide a correct boundary condition for the dangling bonds of the cluster surface atoms because of a lack of information on bonding with atoms outside of the cluster. Creating an artificial molecule with atoms to terminate dangling bonds for peripheral atoms has been only a symptomatic treatment for avoiding troubles. Instead of setting boundary conditions for the cluster, we tried to put the cluster in the model potential, which includes whole local information on an atomlike electronic state in bulk crystal and surface systems. The effective model potential[51-53] $\hat{V}_M$ is constructed by the local potential $V_{\rm loc}$ with orbitals as

$$\hat{V}_M=\Sigma_{\kappa i}\frac{V_{{\rm loc},i}|\Phi_{\kappa,i}\rangle\langle\Phi_{\kappa,i}|V_{{\rm loc},i}}{\langle\Phi_{\kappa,i}|V_{{\rm loc},i}|\Phi_{\kappa,i}\rangle} \ , \quad (12)$$

where subscript i denotes the site of the local potential. In the present paper, the muffin-tin-type potential composed by superimposing atomic charge densities is employed for $V_{\rm loc}$. The local wave function Φ_κ, therefore, is given by the linear combination of the so-called *phi* and *phi-dot* as the eigenfunction of the isolated muffin-tin potential with $\kappa=lm$.[35,36,54,55] Figure 1(b) shows $V_{\rm loc}$ and Φ_κ. Matrix elements for $\hat{V}_M$ are calculated by the same way as those for $V^{\rm ion}_l$ in Eq. (8), using Eq. (6). Since this model potential includes information of the bulklike potential field and bonding property, boundary atoms of cluster having relevance to the bulk crystal are enforced to form a bulklike bond with the model potential, which allows us to pick up surface states within the cluster model.

C. Model

Figure 2 shows the geometrical configuration of the model cluster of CO/$Pt_{13}V_{M37}$ for CO/Pt(111). The molecular axis of CO located on the top site of the center Pt atom is normal to Pt(111).[2,3,12] The 13 black spheres represent Pt and the 37 gray ones surrounding them are V_M. Pt-Pt, Pt-V_M, and V_M-V_M distances are kept fixed at the Pt bulk value, 5.2423 a.u. The local density of states (LDOS) of clean Pt accumulated for 13 Pt sites and

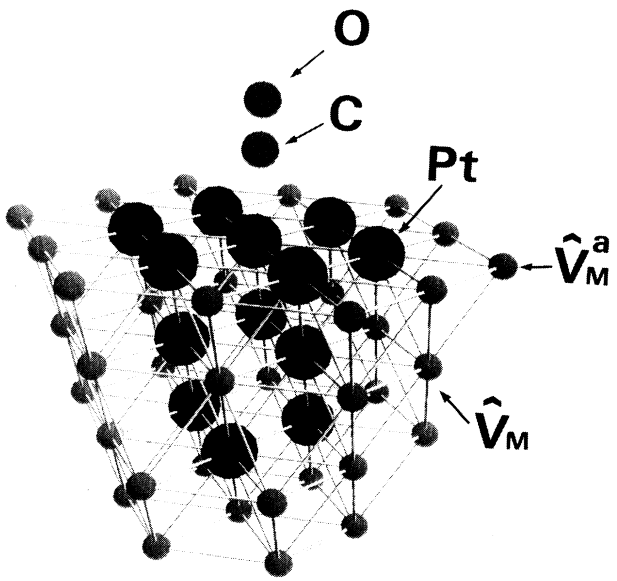

FIG. 2. $Pt_{13}V_{M37}$-CO model cluster for CO/Pt(111). V^a_M and V_M are the model potentials given by Eq. (12). V^a_M indicates the model potential at the surface sites, which is discussed in Sec. IV C as shown in Fig. 11.

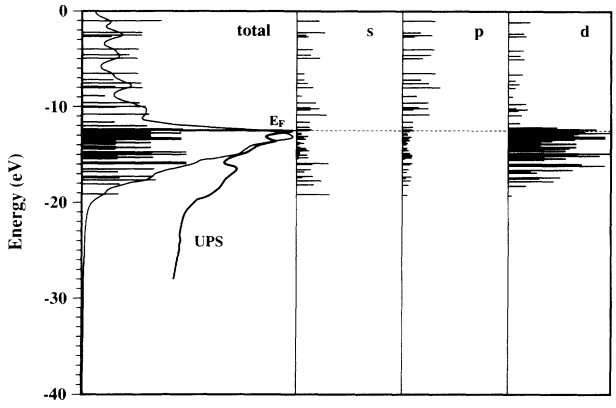

FIG. 3. Total density of states of $Pt_{13}V_{M37}$ cluster and UPS of Pt(111). UPS data are given by Ref. 2. Full curves are obtained by assuming a Lorentzian line shape with 0.5-eV half-width for each line shown in the upper panel.

37 cluster sites for the model potential is shown in Fig. 3, together with the experimental surface (UPS) data.[1,2] The peak around the Fermi level of the LDOS and UPS are in good agreement, which indicates our model potential V_M works to pick up surface states effectively. Figure 4 shows the total energy change of $Pt_{13}CO$ vs Pt-C distance, where the C-O bond length is fixed to 2.132 a.u. The equilibrium distance is about 3.95 a.u. [the metalorganic clusters range is from 3.6 to 3.9 a.u. (Refs. 18 and 21)]. The binding energy at the equilibrium position is about 0.035 hartree given by Eq. (11), where $E_{\rm surf}(Pt_{13}V_{M37})$ and $E_{\rm mol}(CO)$ are -366.858 and -21.420 hartree, respectively. The calculated value is smaller than the experimental data, 0.053 hartree, measured by thermal desorption,[1] which is reasonable because the elongation of the C-O distance increases the binding energy as is discussed in Sec. III A. The stretching frequency given by the curvature of the total energy

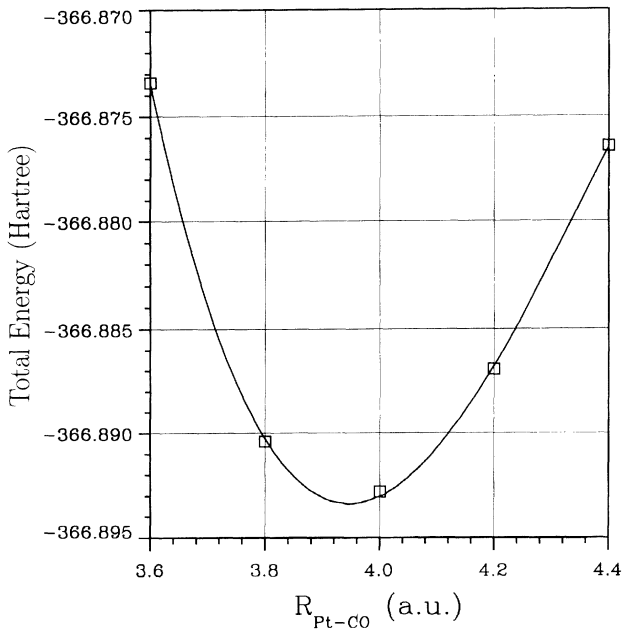

FIG. 4. Binding energy of $Pt_{13}CO$ cluster vs Pt-C distance.

curve is about 494 cm^{-1}, which agrees quite well with the experimental value 468 cm^{-1}.[2,3]

III. ELECTRONIC STRUCTURE

A. Comparison with experiments

Figures 5(a) and 5(b) show the LDOS at Pt and C sites together with the experimental UPS.[1] In this case, Pt-C and C-O distances are kept to be 3.95 and 2.132 a.u., respectively. The contour plots for each molecular orbital on the plane perpendicular to the Pt surface are shown in Figs. 6(a)–6(e). Comparing with those of the free CO allows us to make an assignment of energy levels in the LDOS, as indicated in Fig. 5(b). The global feature of calculated energy levels at both Pt and C sites shown in Figs. 5(a) and 5(b) are in good agreement with the UPS peaks, except the CO-1π orbital, which is deeper than the 5σ one. The angle-resolved UPS data,[4] however, decomposed the broad UPS peak of CO-$5\sigma+1\pi$ to deeper 5σ and shallower 1π states. The reversal of 5σ and π that appeared in the UPS on group-III and Cu metals is due to the elongation of the C-O bond length.[20] Changing the C-O distance into 2.3 a.u. induces the reversal of these levels. Figure 7(a) shows total energy change against the C-O distance, in which the Pt-C distance is kept constant to the equilibrium value, 3.95 a.u. The induced binding-energy increase, being about 0.045 hartree,

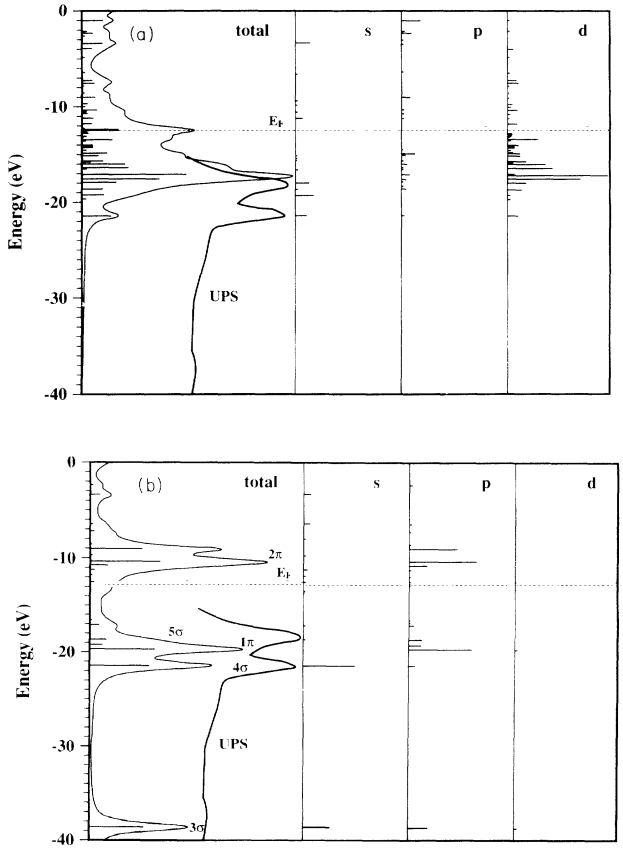

FIG. 5. Same as Fig. 3 for $Pt_{13}CO$ cluster together with UPS of CO on Pt(111) (Ref. 1). (a) On Pt site, (b) on C site.

is two times larger than the expected value estimated from the experimental data, as was discussed in Sec. II C. The stretching frequency of C-O on Pt given by the curvature is 1830 cm^{-1}, which is close to the experimental data, being 1870–2110 cm^{-1}.[2,3] Although the binding energy in the present system is very sensitive to fine details of several factors, such as the numerical errors, the local-density-functional approximation, and basis-set effects, our calculated results are reasonable enough to discuss electronic structures of CO/Pt(111).

The LDOS at the C site with the C-O distance 2.4 a.u. is shown in Fig. 7(b). Calculated energy levels agree very well with the UPS peaks. The CO-5σ and 1π states are found to be very sensitive to the C-O distance. By comparing the LDOS of the Pt site with that of the C site, the character of CO-metal bonding can be comprehended. The LDOS peaks existing below the Fermi level on both sites are CO-5σ and CO-4σ. The unoccupied CO-2π lies about 2–4 eV above the Fermi level, which was not influenced by the Pt-C distance. With adsorbed CO, the 2π-derived level has been reported by bremsstrahlung isochromat spectroscopy to be placed above the Fermi level at 2.7 eV (Ni), 3.4 eV (Cu), and 4.8 eV (Pd), and also reported by the inverse photoemission at 4.3 eV (Pt), 4.6 eV (Pd), and 0.9 eV (Ru).[5–7]. The calculated 2π level is closer to the Fermi level than these data generally. However, it is certain that the Pt-C bond is formed by the interaction between CO-4σ, 5σ, and Pt-5*d*, 6*s*. Co-2π does not contribute to the bonding. Our calculation did not support Blyholder's donation–back-donation model.

Table I shows Mulliken charges of C, O, and the center Pt sites of a $Pt_{13}CO$ cluster with varied Pt-C distances. The CO molecule is almost electrically neutral. This also supports the absence of the charge back-donation to CO

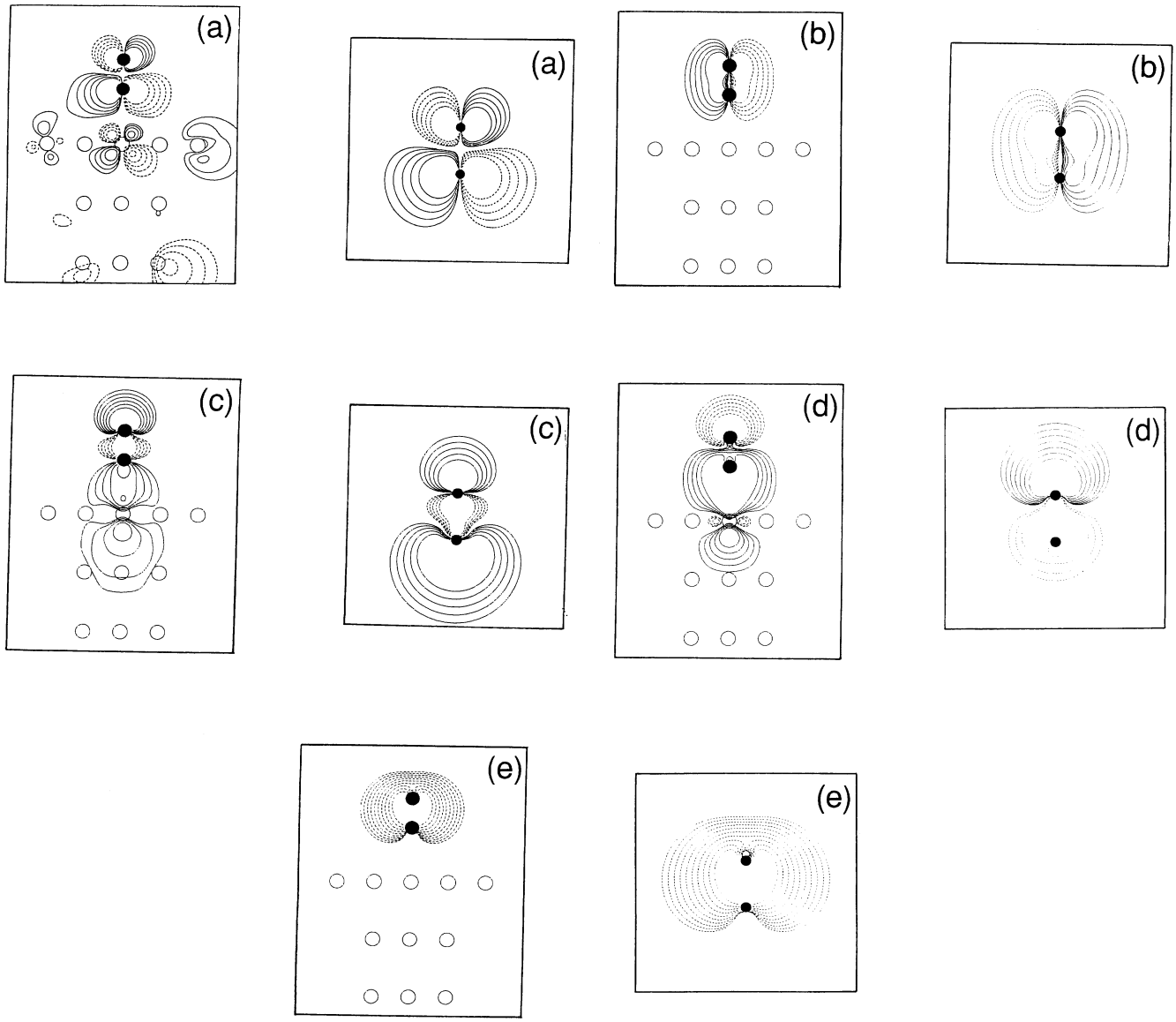

FIG. 6. Molecular orbital of $Pt_{13}CO$ and free CO. Solid and dotted lines are positive and negative values, respectively. (a) 2π, (b) 1π, (c) 5σ, (d) 4σ, (e) 3σ.

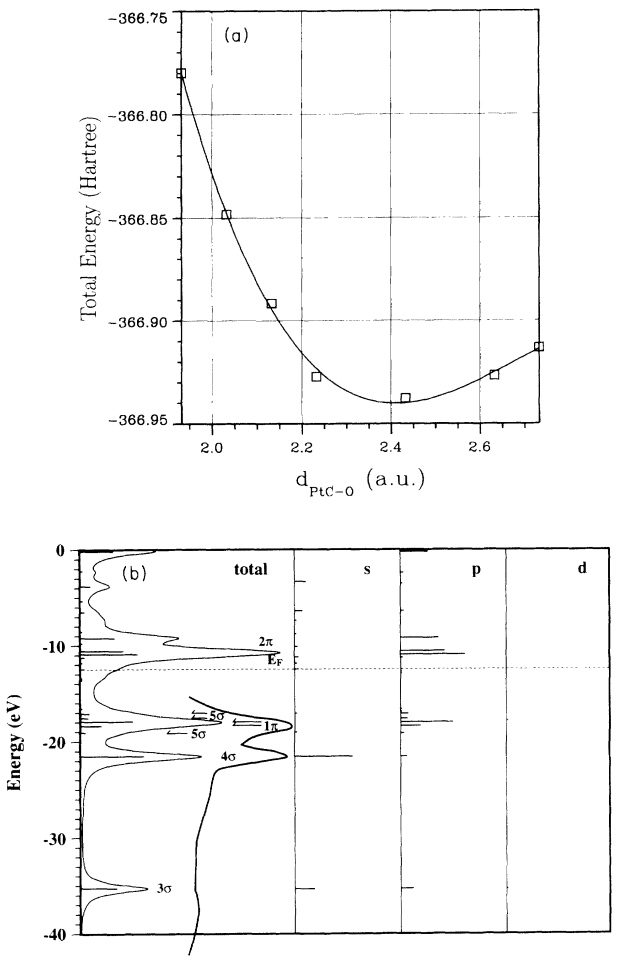

FIG. 7. (a) Total energy curve of $Pt_{13}CO$ cluster vs C-O distance. (b) LDOS of C site of $Pt_{13}CO$ when C-O bond length is elongated. The others are the same as Fig. 3.

from Pt. The LDOS and the UPS indicate that no prominent state exists around the Fermi level of CO adsorbed on the Pt surface. The characteristic molecular orbital of free CO, 2π, 5σ, 1π, 4σ, and 3σ, maintain their original shapes of wave function when CO adsorbs onto Pt. The primary factor of the weak, delicate Pt-CO bond is Pt-5*d* electrons, since the great portion around the Fermi-level states is constructed from them. The mechanism of adsorption, unlike a general covalent bond of a molecule, seems not to be illustrated with a simple model such as the donation–back-donation one.

TABLE I. Mulliken charge, the number of electrons to be associated with the center Pt, C, and O site of $Pt_{13}CO$ cluster with varied Pt-C distance (noted by R). R (Pt-C) bond distances are in atomic units. C+O means the sum of the C site and the O site.

R	Charge of site			
Pt-C (a.u.)	Pt	C	O	C+O
3.6	9.88	3.86	6.23	10.09
3.8	9.92	3.82	6.22	10.05
4.0	9.94	3.78	6.22	10.00
4.2	9.95	3.76	6.22	9.98
4.4	9.93	3.73	6.23	9.96

B. Spin-orbit coupling

In discussions of the energy levels of heavy metal systems like the Pt surface, the spin-orbit effects cannot be ignored. The nonlocal angular-momentum-dependent potential $V_l^{\text{ion}}(r)$ in Eq. (2) is defined as an average pseudopotential of the different $j=l\pm\frac{1}{2}$ states, and the spin-orbit-interaction potential V_l^{so} is given by the difference of the j-dependent potentials.[34] Applying the parameters of Bachelet, Hamann, and Schluter,[34] we can evaluate effects of the spin-orbit interaction on Pt surface states using the same calculation method as Eqs. (6) and (7) by the augmentation of the molecular orbital Ψ_v,

$$P_{vi,lm}(r_i)=\int \Psi_v(\mathbf{r})Y_{lm}(\mathbf{r}_i)d\Omega_i \ , \quad |\mathbf{r}_i|\le R_{\max} \ , \tag{13}$$

where the subscript i indicates the atomic site on which the pseudopotential is located. $\mathbf{r}_i=\mathbf{r}-\mathbf{R}_i$. $r_i=|\mathbf{r}_i|$. $R_{\max}$ is the same as the case of $\hat{V}_l^{\text{ion}}$ in Eq. (6). C-O and C-Pt bond lengths are fixed at 2.132 and 4.0 a.u., respectively. The maximum spin-orbit splitting ξ_{vl} of each molecular orbital v is calculated by the same treatment as Eq. (8). The main contribution comes from the Pt 5*d* state,

$$e_{vi,l}=\Sigma_m \int P_{vi,lm}(r)V_l^{\text{so}}(r)P_{vi,lm}(r)r^2dr \ , \tag{14}$$

$$\xi_{vl}=\Sigma_i e_{vi,l} \ . \tag{15}$$

Table II shows the values of ξ_{vd} for eigenstates around the Fermi level. There are 12 eigenstates between the or-

TABLE II. The estimation of spin-orbit interaction strength ξ_{vd}.

Energy (hartree)	v (No. of orbital)	ξ_{vd} (hartree)
−0.381 19	41,42 (2π)	0.010 09
−0.389 55	43	0.023 50
−0.396 11	44,45	0.014 29
−0.414 87	46	0.022 16
−0.434 29	47	0.016 90
−0.437 94	48	0.023 53
−0.446 02	49	0.022 81
−0.449 25	50	0.022 81
−0.449 88	51,52	0.019 89
−0.454 92	53,54 (LUMO)	0.019 15
−0.456 42	55,56 (HOMO)	0.020 71
−0.458 99	57	0.021 24
−0.460 92	58,59	0.021 30
−0.461 08	60	0.021 93
−0.463 39	61	0.021 55
−0.466 11	62,63	0.021 28
−0.472 79	64,65	0.020 98
−0.475 80	66,67	0.019 09
−0.476 52	68,69	0.020 24
−0.480 54	70	0.020 22
−0.482 18	71,72	0.020 02
−0.485 35	73,74	0.020 28

bital number 49 and 61, of which the energy difference is 0.0174 hartree, while the average of the strength of spin-orbit splitting is 0.02 hartree. It obviously leads to switching highest-occupied molecular orbitals (HOMO) and lowest-unoccupied molecular orbitals (LUMO). However, the 2π level of CO adsorbed on Pt, which lies at 0.075 hartree above HOMO, is split by 0.01 hartree, namely, half of the others because of the orbital localization on CO sites. It implies that the CO-2π state cannot sink under the Fermi level when spin-orbit effects are included.

IV. DISCUSSIONS

Since our calculated result indicates that there is almost no interaction between the CO-2π orbital on the top site of the Pt(111) surface, it is of importance to investigate other possible factors that may affect the bonding nature between CO and Pt surface atoms.

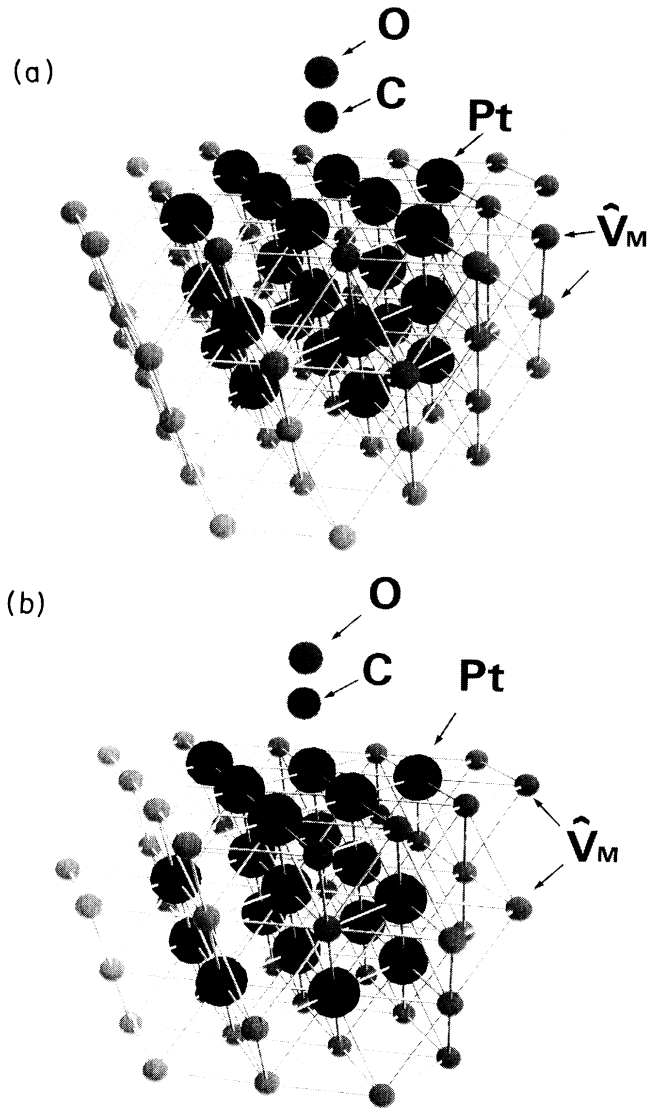

FIG. 8. (a) $Pt_{22}V_{M52}$-CO model cluster for bridge-site adsorption. (b) $Pt_{19}V_{M42}$-CO model cluster for hollow pocket-site adsorption.

A. Site dependence

Since the σ bonding may be strong enough to dominate the whole bonding nature in the case of the top-site adsorption, the size dependence of electronic structures are studied for the bridge and hollow pocket sites with model clusters of $Pt_{22}V_{M52}$ and $Pt_{19}V_{M42}$ as shown in Figs. 8(a) and 8(b), respectively. Figure 9 shows LDOS's at the C site for three cases. It is striking that the Fermi levels in the three model clusters were not essentially changed, which indicates that the present effective-model-potential approach overcomes the difficulties of both size and geometry dependencies in the cluster-model study in this subject. The main CO-2π peak is not affected by the change of the adsorption site. In the bridge-site case, splitting of the 2π orbital occurs because of the bonding with two Pt surface atoms, as expected. The binding energy of the bridge-site case is about 0.04 hartree at the equilibrium distance 2.8 a.u., while that of the pocket-site case is negative at the Pt-C distance 3.2 a.u. CO is not bound at the pocket site as expected.

B. Basis sets

In the norm-conserving pseudopotential scheme, it is not so easy to create additional atomic basis functions by a conventional way, such as the introduction of excited states or external spherical potential well into single atomic-state calculation, which always requires basic modification for V_l^{ps} because of the self-consistent determination of atomic-core states. We fitted radial wave functions to analytical Slater-type ones in order to introduce additional atomic orbitals for the basis function,

$$\chi^*(r)=\Sigma_{(j=1,2)}c_j g_j(r) ,$$
$$g_j(r)=\Sigma_{(j=1,2)}(A_j+rA_{j+3}+r^2A_{j+6})\exp(-\alpha_j r) . \quad (16)$$

Eigenvalues are reproduced to an accuracy of the order of a percent for the relative error. Additional $2s^*$ and $2p^*$ are easily constructed by the Schmidt orthogonalization method by changing coefficient c_j while keeping $g_j(r)$ unchanged. Using these $2s^*$ and $2p^*$ orbitals, we have calculated electronic structures of CO/Pt(111) with the same C-Pt distance as the on-top-site case. Figure 10 compares two electronic structures by minimal and dou-

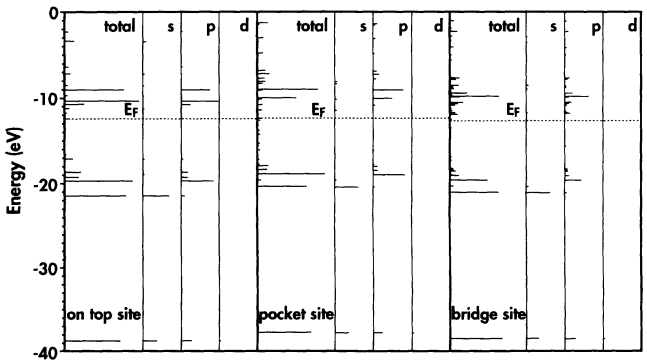

FIG. 9. LDOS's on C sites of Pt-CO clusters for the on-top site, pocket site, and bridge site.

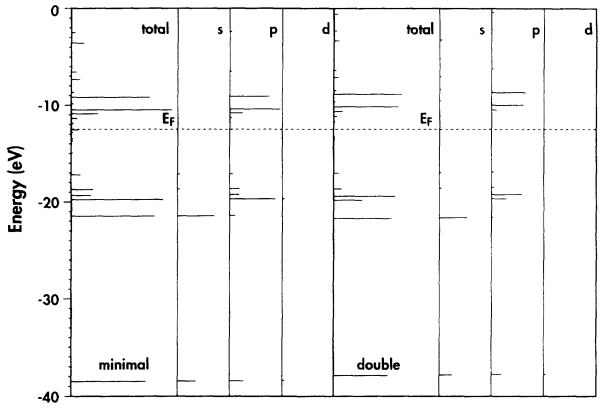

FIG. 10. LDOS's on C site of $Pt_{13}CO$ cluster calculated by minimal and minimal plus additional basis sets.

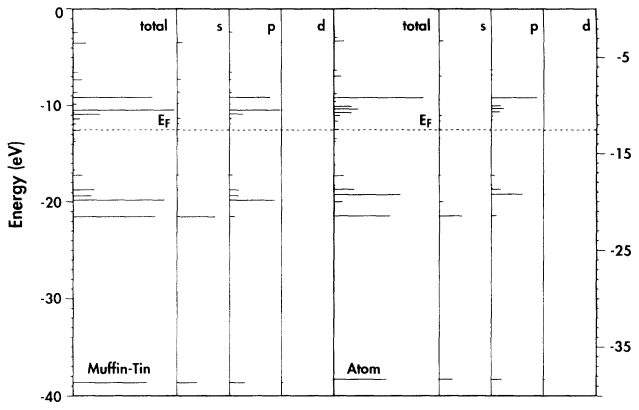

FIG. 11. LDOS's on C site of $Pt_{13}CO$ cluster using muffin tin and atom potential for V_{loc} for cluster sites at the surface region, as shown in Fig. 2.

ble basis functions for CO. 2π orbitals are not so affected by the basis functions while 5σ state splits, which agrees well with the experiments.

C. Model potential

Since the effective model potential $\hat{V}_M$ used so far is the muffin-tin-type one of bulk property, the Pt $6p$ state essentially does not contribute to the projection of molecular orbitals of CO and Pt atoms at the surface. In order to examine the delocalized nature of the CO-2π, 12 V_M's at the surface region shown in Fig. 2, are replaced with the atom model potential constructed by using the atom potential given in Eq. (5) for V_{loc} as

$$V_{loc}=\Sigma_l V_l^{ps}(r)+V_{val}(r) \ . \tag{17}$$

V_{loc} now has the $6p$ open channel for the bound state. Figure 11 shows the LDOS for $CO/Pt_{13}V^a_{M12}V_{M25}$ cluster. Since superimposing the atomic potential energy induces an overestimate of the exchange-correlation potential part, V^a_M introduces the strongest outside potential field into the cluster so that the Fermi level is shifted down by about 5 eV. The CO-2π levels, however, are essentially unchanged by the potential field active for the $6p$ state outside the cluster.

V. CONCLUSION

The LCPSAO-cluster method with the effective model potential for cluster boundary succeeded in picking up the local electronic structure of the CO/Pt(111) system. The calculated CO energy levels on the Pt(111) surface are in good agreement with the UPS data. Since the CO-2π orbital lies above the Fermi level, the back-donation mechanism does not work for CO-Pt bonding.

[1]J. N. Miller, D. T. Ling, I. Lindau, P. M. Stefan, and W. E. Spicer, Phys. Rev. Lett. **38**, 1419 (1977).
[2]P. R. Norton, J. W. Goodale, and E. B. Selkirk, Surf. Sci. **83**, 189 (1979).
[3]P. Hoffmann, S. R. Bare, N. V. Richardson, and D. A. King, Solid State Commun. **42**, 645 (1982).
[4]S. R. Bare, K. Griffinths, P. Hoffmann, D. A. King, G. L. Nyberg, and N. V. Richardson, Surf. Sci. **120**, 367 (1982).
[5]J. Rogozik and V. Dose, Surf. Sci. **176**, L847 (1986).
[6]J. Rogozik, J. Küppers, and V. Dose, Surf. Sci. **148**, L653 (1984).
[7]V. Dose and J. Rogozik, Surf. Sci. **179**, 90 (1987).
[8]A. M. Tobin and P. L. Richards, Surf. Sci. **179**, 387 (1987).
[9]R. Ryberg, Phys. Rev. B **44**, 13 160 (1991).
[10]R. A. Shigeishi and D. A. King, Surf. Sci. **58**, 379 (1976).
[11]H. Steininger, S. Lehwald, and H. Ibach, Surf. Sci. **123**, 264 (1982).
[12]A. M. Baro and H. Ibach, J. Chem. Phys. **71**, 4821 (1979).
[13]S. Lehwald, H. Ibach, and H. Steininger, Surf. Sci. **117**, 342 (1982).
[14]G. Loubriel, T. Gustafsson, L. I. Johansson, and S. J. Oh, Phys. Rev. Lett. **23**, 571 (1982).
[15]R. Murphy, E. W. Plummer, C. T. Chen, W. Eberhardt, and R. Car, Phys. Rev. B **39**, 7517 (1989).
[16]M. D. Baker, N. D. S. Canning, and M. A. Chesters, Surf. Sci. **111**, 452 (1981).
[17]B. Poelsema, L. K. Verheij, and G. Comsa, Phys. Rev. Lett. **49**, 1731 (1982).
[18]A. M. Lahee, J. P. Tonnes, and Ch. Woll, Surf. Sci. **117**, 371 (1986).
[19]G. Blyholder, J. Phys. Chem. **68**, 2772 (1964).
[20]S. Ishii, Y. Ohno, and B. Viswanathan, Surf. Sci. **161**, 349 (1985).
[21]N. K. Ray and A. B. Anderson, Surf. Sci. **119**, 35 (1982).
[22]E. Schweizer, B. N. J. Persson, M. Tushaus, D. Hoge, and A. M. Bradshaw, Surf. Sci. **213**, 49 (1989).
[23]B. N. J. Persson, Phys. Rev. B **40**, 7115 (1989).
[24]G. Volphilhac, M. F. Baba, and F. Achad, J. Chem. Phys. **97**, 2126 (1992).
[25]A. Gavezzotti, G. F. Tantardini, and H. Miessner, J. Phys. Chem. **92**, 872 (1988).
[26]Y.-T. Wong and R. Hoffmann, J. Phys. Chem. **95**, 859 (1991).
[27]H. Ueba, Phys. Rev. B **45**, 3755 (1992).
[28]D. Post and E. J. Baernds, J. Chem. Phys. **78**, 5663 (1983).

[29]P. S. Bagus, K. Hermann, and C. W. Bauschlicher, Jr., J. Chem. Phys. **81**, 1966 (1984).
[30]K. Hermann, P. S. Bagus, and C. J. Nelin, Phys. Rev. B **35**, 9467 (1987).
[31]J. N. Allison and W. A. Goddard III, Surf. Sci. **115**, 553 (1982).
[32]A. C. Pavao, M. Braga, C. A. Taft, B. L. Hammond, and W. A. Lester, Jr., Phys. Rev. B **44**, 1910 (1991).
[33]G. Pacchioni and P. S. Bagus, J. Chem. Phys. **93**, 1209 (1990).
[34]G. B. Bachelet, D. R. Hamann, and M. Schluter, Phys. Rev. B **26**, 4199 (1982).
[35]S. Ohnishi, T. Ikeda, and N. Watari, *Computer Aided Innovation of New Materials* (North-Holland, Amsterdam, 1991), p. 175.
[36]S. Ohnishi, *Ordering at Surfaces and Interfaces,* edited by A. Yoshinori, T. Shinjo, and H. Watanabe, Springer Series in Material Science Vol. 17 (Springer-Verlag, Berlin, 1992), p. 353.
[37]P. Hohenberg and W. Kohn, Phys. Rev. **136**, B864 (1964).
[38]W. Kohn and L. J. Sham, Phys. Rev. **140**, A1133 (1965).
[39]D. M. Ceperley and B. J. Alder, Phys. Rev. Lett. **45**, 566 (1980).
[40]J. P. Perdew and A. Zunger, Phys. Rev. B **23**, 5048 (1981).
[41]A. D. Becke, J. Chem. Phys. **88**, 2547 (1988).
[42]S. L. Sobolev, Sov. Math. **3**, 1307 (1962).
[43]A. D. McLaren, Math. Comput. **17**, 361 (1963).
[44]V. I. Lebedev, Sib. Math. Zh. **18**, 132 (1977).
[45]A. H. Stroud, *Approximate Calculation of Multiple Integrals* (Prentice-Hall, Englewood Cliffs, NJ, 1971).
[46]E. J. Baerends, D. E. Ellis, and P. Ros, Chem. Phys. **2**, 41 (1973).
[47]H. Sambe and R. H. Felton, J. Chem. Phys. **62**, 1122 (1975).
[48]B. I. Dunlap, J. W. D. Connolly, and J. R. Sabin, J. Chem. Phys. **71**, 3396 (1979).
[49]J. Harris, R. O. Jones, and J. E. Muller, J. Chem. Phys. **75**, 3904 (1981).
[50]B. Delley, D. E. Ellis, A. J. Freeman, E. J. Baerends, and D. Post, Phys. Rev. B **27**, 2132 (1983).
[51]S. Weinberg, Phys. Rev. **131**, 440 (1963).
[52]J. B. Pendry, J. Phys. C **10**, 809 (1977).
[53]L. Kleinman and D. M. Bylander, Phys. Rev. Lett. **48**, 1425 (1982).
[54]O. K. Andersen, Phys. Rev. B **12**, 3060 (1975).
[55]O. K. Andersen, O. Jepsen, and D. Glotzel, in *Highlight of Condensed-Matter Theory,* Proceedings of the International School of Physics "Enrico Fermi," Course LXXXIX, Varenna, 1983, edited by F. Bassani, F. Fumi, and M. P. Tosi (North-Holland, Amsterdam, 1985), pp. 59–176.

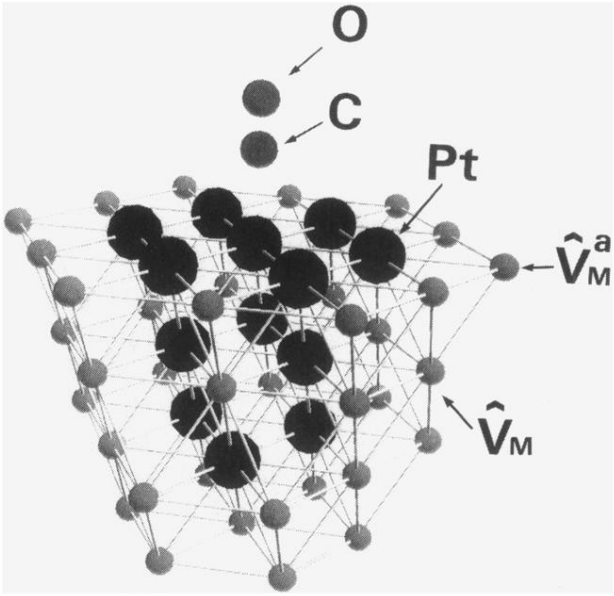

FIG. 2. $Pt_{13}V_{M37}$-CO model cluster for CO/Pt(111). V_M^a and V_M are the model potentials given by Eq. (12). V_M^a indicates the model potential at the surface sites, which is discussed in Sec. IV C as shown in Fig. 11.

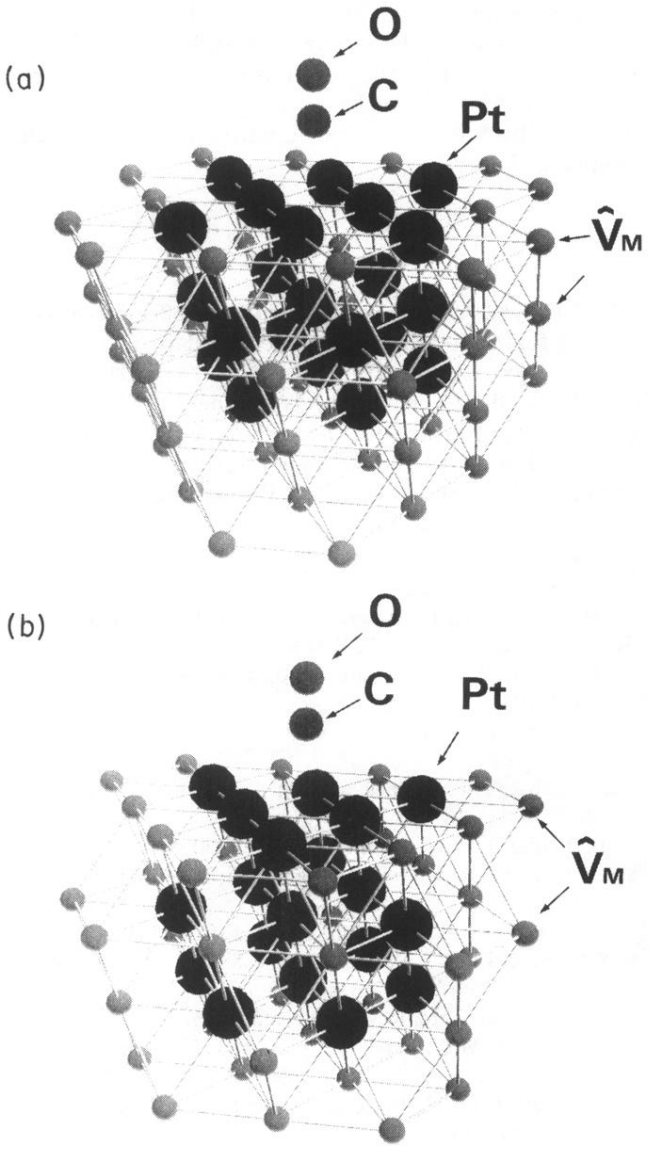

FIG. 8. (a) $Pt_{22}V_{M52}$-CO model cluster for bridge-site adsorption. (b) $Pt_{19}V_{M42}$-CO model cluster for hollow pocket-site adsorption.